Strong inhomogeneity of the tunnel Schottky structures with δ-doped two-dimensional channels at large bias

Michael Feiginov
Technische Universität Darmstadt, Merckstr. 25, D-64283 Darmstadt, Germany

Igor N. Kotelnikov and Nikolay A. Mordovets
Institute of Radioengineering and Electronics, Russian Academy of Sciences, Mokhovaya St. 11, Moscow 101999, Russia
(Received 7 January 2010; revised manuscript received 6 May 2010; published 17 August 2010)

The electron transport in the tunnel Al/GaAs Schottky structures with two-dimensional δ-doped channels is investigated both experimentally and theoretically. We observe experimentally strong inhomogeneity and "freezing" of the potential profile along the channel at large biases. Also, the total current saturates at large biases and the differential resistance shows a characteristic nonmonotonous behavior. A theoretical model for the structures is developed. It is in quantitative agreement with the measurements. The model explains the observed features by the channel depletion and the decrease of its conductivity with bias. Our measurements and theoretical calculations indicate that a local impurity-density-induced transition into insulator state is taking place in our structures, when the electron concentration in the channel is still relatively high ($\approx 3\times 10^{11}$ cm^{-2}). We identify the poor conductivity of the locally depleted part of the channel as the bottleneck leading to the current saturation and to appearance of the other features mentioned above.

DOI: 10.1103/PhysRevB.82.075318 PACS number(s): 73.40.Gk, 73.63.Hs, 73.40.Ns, 73.25.+i

I. INTRODUCTION

The experimental investigation of the tunnel Schottky structures with δ-doped two-dimensional (2D) channel[1–6] has led to demonstration of a number of new effects in the recent years. In particular, the observation of a resonant intersubband polaron interaction,[2] the effect of electron reflection when tunneling into 2D system at the threshold of LO-phonon emission,[3] persistent tunnel photoconductivity,[4] many-body effects,[5] evidences for inherent negative differential conductance (NDC) of the Schottky contacts with 2D channels,[6,7] etc. That makes the structures attractive for fundamental studies and, additionally, some of the discovered effects (e.g., NDC) could turn out to be useful in applications. There are two main reasons that have made the observation of the above effects possible. First, one can apply the tunnel-spectroscopy measurement technique[1,8,9] to such structures. The tunnel spectroscopy has the advantage that one can access both the occupied and empty subbands, in contrast to the usual magnetotransport measurements of the 2D electron systems (see, e.g., Ref. 10), where only the occupied subbands could be characterized. The second reason is the high quality of the tunnel barrier in the Al/GaAs tunnel structures that could be achieved by the *in situ* molecular beam epitaxy (MBE) growth of a metal.[2–6,11–13]

Till now, such tunnel structures have been investigated[1–6] at relatively low biases of $\approx \pm 100$ mV only. Usually, the inhomogeneity of the voltage distribution along the 2D channel under the metal (Al) gate is negligibly small in such regime. The situation is different at larger biases. Here, on one hand, the current density becomes relatively high. On the other hand, at large applied bias the channel might become depleted and poorly conducting. That leads to appearance of the macroscopical inhomogeneities in the voltage and in the electron-concentration distributions along the channel. Additionally, the local tunnel current density is changing exponentially fast with the variation of the local bias across the barrier and that results in strong inhomogeneity of the tunnel current injected into the channel. The factors limit the resolution of the tunnel-spectroscopy method and lead to peculiarities in the *I-V* and other characteristics of the structures. The present paper is devoted to the investigation of exactly this regime and associated peculiarities in the Al/GaAs tunnel structure with δ-doped 2D channel, when large biases are applied.

Additionally, the investigation of the tunnel Schottky structures with 2D channels at large biases is touching to some extend the field of the metal-insulator transition (MIT) in the 2D systems, see, e.g., Ref. 14. When a large bias is applied, the channel becomes eventually enough depleted so that the channel or a part of it might come close to the MIT regime. That happens in our structures. The effects relevant for MIT (channel depletion, large not-screened microscopical potential fluctuations, their nonlinear screening, strong decrease in the channel conductivity) in addition to strong influence of the potential fluctuations on the tunnel current, all these effects are taken place in our structure, they determine the measured characteristics and they should be included in the theoretical analysis of the measurement results. We can also add that the impurity-density-induced MIT in the heavily δ-doped layers (as in our structures) has been addressed, to our knowledge, in just few publications[15,16] in the past.

The paper is organized as follows. We describe the samples and their fabrication procedure in Sec. II. A short description of the general properties and low-bias characteristics of the structures is given in Sec. III. An account of the experimental observations at large biases is given in Sec. IV and the theoretical model for this case, together with the calculation results are described in Sec. V. Conclusions are presented in Sec. VI.

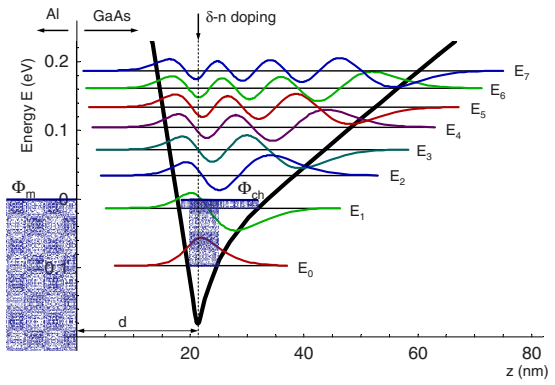

FIG. 1. (Color online) Band diagram of Al/GaAs structure at zero bias, the 2D channel is formed by the δ-n doping at $z=d\approx 20$ nm.

II. SAMPLES

We were using an MBE grown Al/GaAs structure in our experiments. Al was grown in MBE *in situ* to achieve high quality of the metal/semiconductor interface. δ-n-layer with the doping level of $\approx 7\times 10^{12}$ cm^{-2} was grown at the distance of 20 nm from the Al/GaAs interface. The whole structure was p-doped at the level of $\sim 10^{16}$ cm^{-3}.

The δ-n-layer forms a narrow 2D electron channel with a steep Schottky barrier on one side and a relatively gentle sloping on the side of the deep GaAs layers. Due to the relatively high p doping, the channel is quite narrow and the separation between 2D subbands is ~ 50 meV. The Schottky barrier of the structure is quite thin and the electrons can tunnel through it. Two subbands are occupied in the 2D channel of our samples at zero bias. The calculated band diagram of the structure is shown in Fig. 1.

The Al gates with different geometries were defined and the Ohmic contacts were fabricated on the wafers afterwards. The samples were prepared in the form of Hall bars with the width of the 2D channel of 0.5 mm and the full length of 1.5 mm. We had two types of samples, see Fig. 2. One is with two tunnel gates of the length of 10 μm close to the ends of the Hall bar (sample "d"), the another one (sample "e") had practically the whole Hall bar covered by the Al gate, the gate length was 1.3 mm in this case. The rho contacts were between the two gates in the first case and contacting the channel under the gate in the second one. The distance between the gate edges and the nearest Ohmic (current) contacts was 100 μm for both types of structures. Owing to the rho contacts, we could measure the potential distribution at several points under the gate of sample e, when the bias is applied between the gate and the current (drain) Ohmic contact.

III. LOW-BIAS BEHAVIOR

A. Experimental observations

The tunnel spectrum of the structure d with short gate measured at low biases at 4.2 K is shown in Fig. 3. The tunnel spectrum is the second derivative of the current, normalized by the conductance (σ). At low biases, when the

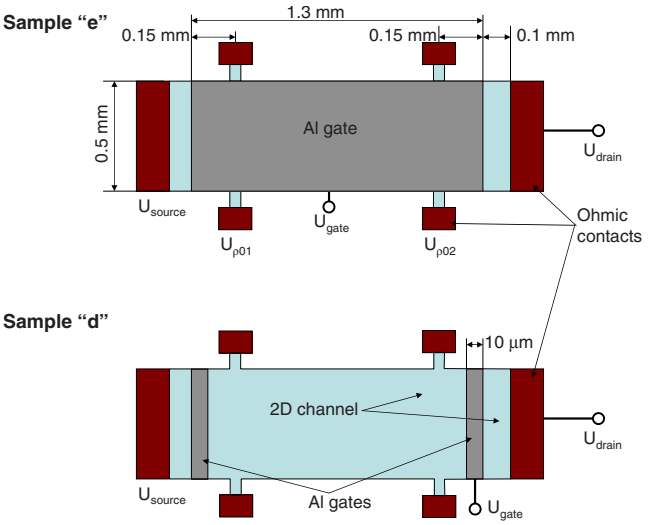

FIG. 2. (Color online) Sample geometries. The samples had the geometry of the Hall bars with the same dimensions, except for the length of the Al gates. The gate was covering almost the whole bar in the case of sample e and only narrow stripes close to the ends of the bar in the case of sample d. The bias is applied between the gate and the drain Ohmic contact whereas the source contact is kept open.

inhomogeneity of the voltage distribution in the channel is negligibly small, the interpretation of the spectra is straightforward:[8,9] the minima in the spectrum correspond to the bias points, where the metal (Al) Fermi level crosses the bottoms of the 2D subbands in the channel. By measuring the spectrum, one gets the energy position of the bottoms (E_i) of the filled as well as empty subbands.

The spectrum minima at the negative biases give us the energy positions of the bottoms of the two filled subbands, they are $E_0\approx -120$ meV and $E_1\approx -20$ meV for the ground and first excited subbands, respectively. The subband bottom energies are related to the electron concentration in the subbands via 2D density of states. Independently, we have also measured the Hall electron concentration of $\approx 3.1\times 10^{12}$ cm^{-2} in the channel under the gate in the sample e. The δ-layer conductivity (at 4.2 K) of the gated

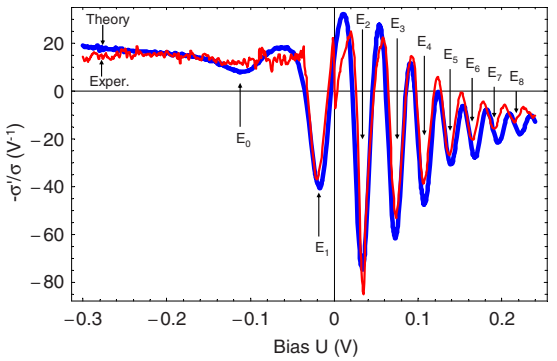

FIG. 3. (Color online) The tunnel spectrum $-d[\ln(\sigma)]/dU$ measured at low biases at $T=4.2$ K for d sample and the results of the self-consistent calculations. The arrows indicate the positions of the subbands: $E_0\approx -120$ meV, $E_1\approx -20$ meV, etc.

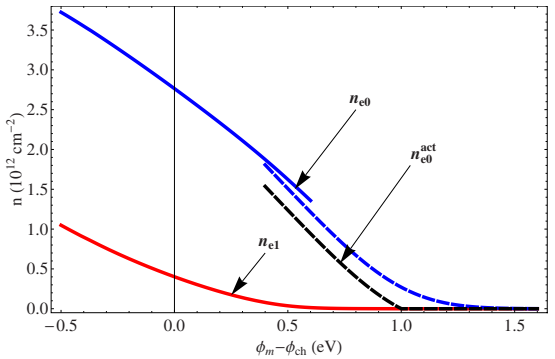

FIG. 4. (Color online) The calculated electron concentrations n_{e0} and n_{e1} in the lowest two subbands E_0 and E_1, respectively, at different voltages. The continuous lines show the plots calculated with low-bias model, the dashed lines are calculated with large-bias model. n_{e0}^{act} is an active electron concentration above the percolation threshold. Φ_{ch} is the channel Fermi level, Φ_m is the Fermi level in the Al gate. If one would neglect by the macroscopical inhomogeneities, then the bias (U) applied to the structure is related the Fermi-level difference as $eU=\Phi_m-\Phi_{ch}$.

channel at zero bias was measured to be 0.28 mS/□ (mS per square), that gives us the subband mobilities of $\mu_0^0=500$ cm^2/Vs and $\mu_1^0=800$ cm^2/Vs for the ground and first-excited subbands, respectively, at zero bias. We used the tunnel data (Fig. 3) for such estimations of mobilities: the electron concentration in the two filled subbands in the gated areas of the structure at zero bias are $\approx 2.8\times 10^{12}$ cm^{-2} and $\approx 4\times 10^{11}$ cm^{-2} for the subbands E_0 and E_1, respectively, see Fig. 4. Although the minimum of the ground subband is not clearly recognizable in the spectrum in Fig. 3, the value of the Hall electron concentration unambiguously indicate that the slight minimum in the spectrum at ≈ -120 mV marked as E_0 subband in Fig. 3 corresponds to the filled ground subband in the channel. Additionally, the Hall measurements with the sample d, where almost the whole Hall bar was not covered by the gate, show that the electron concentration in the not-gated parts of the channel is somewhat lower than under the gate, it is $\approx 2.4\times 10^{12}$ cm^{-2}. The δ-layer conductivity was 0.15 mS/□ in this case.

B. Theoretical calculations

Further, the band structure of our samples was calculated self-consistently in the Hartree approximation, nonparabolicity was taken into account in the two-band approximation.[17] In the calculations, the δ-n-layer was assumed to be at the distance of 21.2 nm from the Schottky contact, the distance is close to the nominal MBE-growth value of 20 nm. The Schottky-barrier height at Al/GaAs interface is ≈ 0.9 eV at the liquid-helium temperature, as determined with the specially grown Al/n-GaAs structures with homogeneous n doping and using a method relying on tunnel I-V measurements.[18] The barrier height is in agreement with the other literature data,[19,20] where the value of ≈ 0.8 eV at room temperature has been reported for the *in situ* grown Al/GaAs. The levels of δ-n doping (7.2×10^{12} cm^{-2}) and p doping (1.2×10^{16} cm^{-3}) in our structure were determined by fitting of the subband minima in the calculated and measured spectra (see Fig. 3), the values are in reasonable agreement with the nominal MBE growth parameters. When calculating the tunnel spectra, the fitting of the subband broadening and comparison of the minima width in the calculated and measured spectra gives us information about the broadening of the different subbands, they were determined to be $\Delta E_0 \approx 17$ meV (half width) and $\Delta E_1 \approx 7$ meV for the filled ground and first excited subbands, respectively, and it was growing from $\Delta E_2 \approx 5$ meV to $\Delta E_{14} \approx 9$ meV for the empty higher subbands. The broadening of the lowest two subbands is in good agreement with the measured mobilities in the subbands at zero bias. The additional peaks and minima one can see in the measured spectra in Fig. 3 are due to the zero-bias anomaly (at ≈ 0 V) and phonon-assisted tunneling (at $\approx \pm 36$ mV).[1–3,5]

We note here that, generally speaking, the positions of the subband bottoms at zero bias do not correspond exactly to the bias points ($\times e$, here e is the electron charge) of the minima in the spectrum. The deviation in our structures is typically $\sim 10\%$ of the bias points ($\times e$) of the minima: the subbands in the channel are shifting slightly with respect to the channel Fermi level, when the bias is changing. The shift is due to the change in the electron concentration in the channel and also due to small variation in the channel profile with bias. The latter effect is usually much smaller than the first one in our structures. If the electrons fill the ground subband (E_0) in the channel only, then one can write a simple relation between the variation in E_0 with respect to the channel Fermi level (Φ_{ch}) and the variation of the gate-channel Fermi-level difference (Φ_m is the Fermi level in the gate)

$$\delta E_0 \approx \frac{1}{\beta}\delta(\Phi_m - \Phi_{ch}), \tag{1}$$

$$\beta = \frac{e^2\rho_{2D}}{C}, \tag{2}$$

where $C=\varepsilon/4\pi d$ is the specific gate-channel capacitance, ε is the lattice dielectric constant in the Schottky barrier, d is the Schottky-barrier thickness (the separation between the δ layer and the metal gate) and ρ_{2D} is the 2D density of states in a channel subband. The unitless factor β

$$\beta \approx 8 \tag{3}$$

for our structures. To correct for the above variations and to determine the subband positions at zero bias with an accuracy better than 10% from the measured spectrum, one can use an approximate correction in Eq. (1) and the relation $\delta E_i \approx \delta E_0$, where δE_i are the shifts of the bottoms of the excited subbands with bias, or, more accurately, one has to compare the measured spectra with the self-consistent calculations, as we have done that above in Fig. 3.

C. Inhomogeneities in the low-bias regime

The macroscopical inhomogeneities in the voltage distribution along the channel might become important even in the low-bias regime. The conductivity of the channel is not infi-

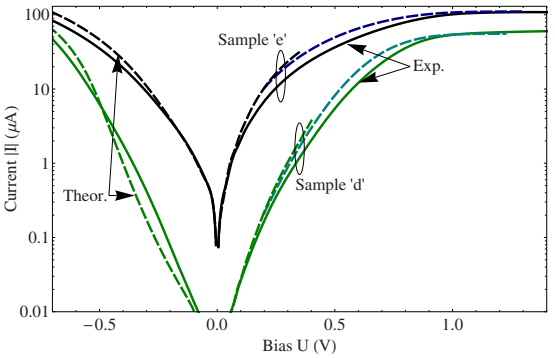

FIG. 5. (Color online) Calculated (dashed lines) and measured (continues lines) *I-V* curves of the sample e and d. The dashed lines at $U \gtrsim 0.3$ eV are calculated with the large-bias model, the dashed lines at lower biases are calculated with the low-bias model.

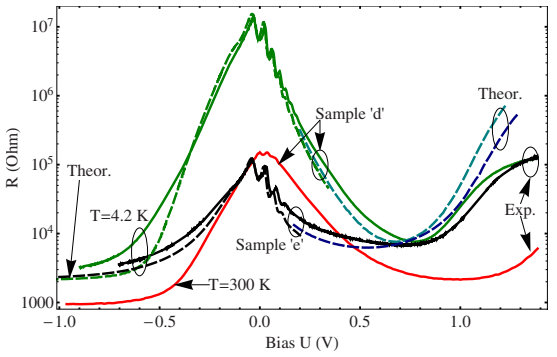

FIG. 6. (Color online) Voltage dependences of the differential resistance ($\partial U/\partial I$) for the d and e samples. The continuous and dashed lines are the experimental and theoretical curves, respectively. One line ($T=300$ K) shows the measurements of the sample d at room temperature. All the other curves show measurements and calculations at 4.2 K. The dashed lines at $U \gtrsim 0.3$ eV are calculated with the large-bias model, the dashed lines at lower biases are calculated with the low-bias model.

nitely high, therefore an inhomogeneity of the voltage distribution in the channel appears with increase in the current flowing through it. In its turn, the tunnel current is growing exponentially with increase of the bias applied to the structure. Already at relatively low biases, the voltage drop along the channel under the gate (ΔU_{ch}) might become comparable to the width of the spectral features in the tunnel spectrum. At this point, the inhomogeneities become a limiting factor of the tunnel spectroscopy method. ΔU_{ch} is given by the following expression for a channel with a position-independent conductivity:

$$\Delta U_{ch} = \frac{j_t}{\sigma_0}\frac{L^2}{2}, \tag{4}$$

where L is the length of the gate, j_t is the density of the tunnel current, σ_0 is the conductivity of the channel at zero bias. As mentioned above, the measured value of σ_0 is equal to 0.28 mS/□ in our samples. The measurement data for j_t show that ΔU_{ch} becomes comparable to the width of the minima in the tunnel spectrum (~10 mV) already at ~50 mV for the sample e. One can see that the inhomogeneities can limit the resolution of the tunnel spectroscopy already at pretty low biases in the structures with relatively long gates. In the opposite case of the sample d, where the gate is short, ΔU_{ch} is less than 1 mV for the biases in the range of ±0.5 V. Equation (4) shows that the limitation of the energy resolution of the tunnel spectroscopy method drops as L^2 with decrease of the length of the gate.

IV. LARGE-BIAS BEHAVIOR, EXPERIMENT

The experimentally measured *I-V* curves and the differential-resistance characteristics of the samples e and d in a wide range of applied biases are shown in Figs. 5 and 6. One can see that the *I-V* curves and the differential resistances have some peculiar features at large positive biases. The currents saturate at around 0.9 V for both samples and the differential resistances of the structures at positive (channel-depleting) biases have distinctly nonmonotonous behavior: they are first decreasing with bias, then they reach a minimum at around 0.8 V and finally they are increasing. At negative (channel-enriching) biases the structures behave in a rather expectable way: the current saturation does not appear and the differential resistance is steadily decreasing with bias for both samples. At high negative biases, the differential resistance comes to a saturation at the value equal to ≈2 kOhm at 4.2 K, that corresponds approximately to the resistance of 1.5 kOhm of the open part of the channel between the Ohmic contact and the gate.

The differential resistance of the structure d measured at room temperature (see Fig. 6) looks qualitatively similar to that measured at low temperature apart from two differences. One is that the differential resistance lowers significantly at room temperature by around 1–2 orders of magnitude at low and positive biases and the saturation differential resistance at the negative biases (the resistance of the nongated part of the channel) is a factor of two lower than that at low temperature. The second difference is that the subband features at low biases are almost washed away at room temperatures because of the thermal broadening of the Fermi distribution.

In our structures, we could also probe the voltage at the other side of the channel at the second current Ohmic (open "source") contact (see Fig. 2) and additionally we could probe the voltage at the rho contacts under the long gate of the structures of the type e. The voltages at the open Ohmic and the rho contacts vs applied bias are shown in Fig. 7. One can see that the voltages saturate with increase of the applied bias. The saturation of the voltages indicates "freezing" of the voltage distribution under the gate, which is taking place in the current-saturation regime at the biases above ≈0.9 V. Also one can see large inhomogeneity of the voltage distribution under the gate of sample e in the current-saturation regime: the voltage difference between the two rho contacts is around 0.2 V for the sample. The voltages at the open Ohmic contact (source) and the contact $\rho 01$ are almost coinciding in the sample e. Such behavior is explained in the next section.

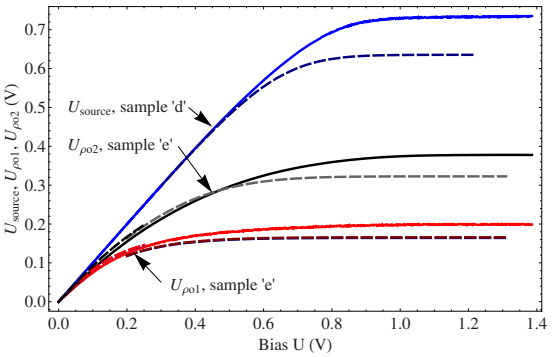

FIG. 7. (Color online) The dependences of the voltages at the open source contact of the sample d and at the rho contacts of the sample e vs applied bias. The source voltage of the sample e practically coincides with the voltage at the $\rho 01$ contact. The continuous and dashed lines show the experimental and theoretical curves, respectively. The dashed lines at $U \gtrsim 0.3$ eV are calculated with the large-bias model, the dashed lines at lower biases are calculated with the low-bias model.

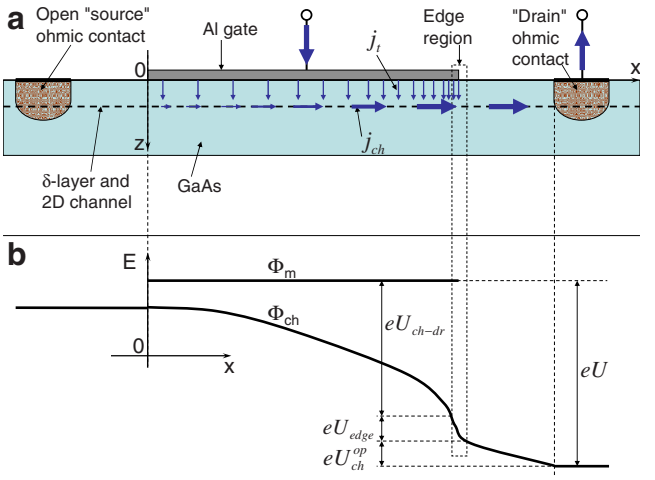

FIG. 8. (Color online) (a) The schematic shows the channel current and tunnel currents in the structure and (b) also the profiles of the Fermi levels in the channel and gate.

V. THEORETICAL MODEL FOR LARGE-BIAS REGIME

A. Qualitative model

One can suggest an analogy to a high-electron-mobility transistor (HEMT) to explain the operation of the tunnel structures in the regime of large biases. At high voltages at the drain of a HEMT (see, e.g., Ref. 21), the channel under the gate starts to be depleted, especially at the drain side of the gate. The electric field along the channel is increasing there, at some point it reaches the level, when the electron drift velocity in the channel saturates, that leads to the saturation of the total current of the HEMT. At even higher biases at the drain, the current stays basically constant and the potential distribution in the channel under the gate is freezing. If one takes a derivative of the current and plots the source-drain differential resistance as a function of the source-drain voltage, then the differential resistance will be low at low voltages. Then the resistance will be increasing with bias and, ideally, it should be diverging, when the current at the drain side of the channel comes to a saturation. Looking at the distribution of the voltage in the channel of HEMT in the saturation regime, one should see that the voltage is smoothly changing going from the source in the direction of the drain, then the voltage is changing more and more rapidly, the more channel is depleted, and finally the voltage exhibits an almost steplike jump in the depleted part of the channel under/near the drain side of the gate.

The tunnel structures, that we are investigating in the present work, behave in a similar fashion. The major difference is that the current is not supplied by the source contact (it is open), as in HEMT. Instead, the tunnel current is injected into the channel from the gate (at the channel depleting biases). At low gate-drain biases, the drain current in our structure is exponentially increasing with bias due to the increase in the tunnel current under the whole area of the gate. With further increase in the bias the inhomogeneities appear because, on one hand, the channel current is growing. On the other hand, the electron concentration in the channel drops (inhomogeneously) and therefore the channel conductivity is decreasing. At some point these two effects lead to appearance of a strong electric field along the channel, especially under the drain edge of the gate, where the channel current has a maximum and the electron concentration has a minimum. That causes the electron velocity in the channel under the drain edge of the gate to saturate. When that happens, then, ideally, that should lead to the saturation of the total current of the structure (cf. Fig. 5). The voltage distribution and the electron concentration in the channel under the gate, the distribution of the tunnel-current density should "freeze" and stay constant (cf. Fig. 7), when higher biases are applied to the structure. We see that the mechanism of the current saturation is completely analogous to that in HEMTs.

If we take a derivative of the current and take a look at the voltage dependence of the gate-drain differential resistance of our tunnel structure, then the differential resistance should be decreasing with bias at low biases (cf. the range $0 < U < 0.8$ V in Fig. 6), rather than staying constant as in HEMTs. That happens due to a roughly exponential increase of the tunnel conductivity of the tunnel Schottky barrier with bias. At higher biases, at the transition to the current-saturation regime, the gate-drain differential resistance should be increasing (cf. the range 0.8 V $< U$ in Fig. 6) and, ideally, diverging. In such a way we see that the differential resistance of our structures should have a characteristic minimum at some bias ($U \approx 0.8$ V in Fig. 6), corresponding to appearance of the channel depletion.

In reality, the characteristics of the tunnel structures are not ideal and the current does not come fully to a saturation. This is due to the fact that the gate-channel voltage changes with bias in the depleted part of the channel under the gate edge and that gives rise to an additional tunnel current injected into the depleted part of the channel, see Fig. 8. Although spatially the channel depletion region is usually small as compared to the total gate area, the tunnel current density is exponentially high there. Because of that, this "edge" current might give an appreciable contribution to the total current. In result, the gate-drain differential resistance does not

diverge in the large-voltage regime (see Fig. 6). Nevertheless, the voltages at the source and rho contacts under the gate should still come to a saturation at large biases since the edge effects should not affect the freezing of the potential distribution in the deep parts of the channel under the gate (cf. Fig. 7).

To verify the qualitative picture above and its agreement with the measurements, we have developed a quantitative model for the large-bias regime. We consider two types of inhomogeneities in our structures. One is macroscopical inhomogeneities conditioned by the current flow. The other one is microscopical inhomogeneities due to the fluctuations in the doping concentration in the channel. Contrary to conventional HEMTs, the channel of our structures is heavily doped and the inevitable microscopical fluctuations of the dopant density lead to large-amplitude potential fluctuation in the channel. In its turn, the potential fluctuations have an impact on the local and average tunnel current injected into the channel from the gate. A model, which takes into account the microscopical potential fluctuations in the channel, their screening by the gate and by the channel electrons, percolation effects and their impact on the electron mobility in the channel, the tunnel-current fluctuations and also the macroscopical inhomogeneities, is described in the subsequent sections.

B. Nonlinear screening of charge fluctuations

The objective of this section is to determine the microscopical potential fluctuations and the averaged electron concentration in the channel in the presence of the donor-density fluctuations. Let us consider a δ-doped 2D layer with an average 2D dopant density of N_D. The dopant atoms are randomly distributed along the 2D layer, we assume here that the dopants are located exactly in the plain of the δ-layer only. The probability of finding X atoms in an area S of the 2D layer is described by the Poisson distribution

$$P(X,S) = \frac{(N_D S)^X}{X!}\exp(-N_D S). \tag{5}$$

Assuming that

$$X \gg 1, \tag{6}$$

treating $X=N_D^{loc}S$ as a continues variable (N_D^{loc} is a local donor density averaged over an arbitrary-chosen area S) and assuming that

$$|N_D^{loc} - N_D| \ll N_D \tag{7}$$

we can replace the Poisson distribution in Eq. (5) by the Gaussian one

$$P_{ND}(N_D^{loc}) \simeq \frac{1}{\sqrt{2\pi}\eta_{ND}}\exp\left[-\frac{(N_D^{loc}-N_D)^2}{2\eta_{ND}^2}\right], \tag{8}$$

where η_{ND} is the standard deviation

$$\eta_{ND} = \frac{\sqrt{N_D}}{\sqrt{\pi}r}, \tag{9}$$

if we take the area S in the form of a circle of a radius r.

The donor-density fluctuations lead to fluctuations in the channel-bottom potential. Such fluctuations will be screened by two mechanisms. One is screening by the gate, this screening mechanism is always present and it is linear. The second one is the screening by the electrons in the channel, which is taking place in the regions of the channel filled by electrons (below the Fermi level) only, i.e., this is a nonlinear mechanism. Further we calculate the potential fluctuations with the account of both screening mechanisms.

We assume that the fluctuations of N_D^{loc} have a fixed radius r (the radius will be defined later on), which satisfies the condition

$$2r \gtrsim d. \tag{10}$$

Assuming that the charge is distributed homogeneously inside the fluctuations of radius r and because of the condition in Eq. (10), we can apply the local-capacitance approximation

$$\delta\varphi_{ch} = \frac{e^2}{C}(\delta n_{e0}^{loc} - \delta N_D^{loc}), \tag{11}$$

where n_{e0}^{loc} is the local electron concentration in the channel and φ_{ch} is the electron potential energy at the channel bottom. The approximation allows us to treat both the gate and electron screening in a simple fashion.

Let us assume that the channel is filled by electrons till a Fermi level (Φ_{ch}). By N_0 we denote a donor density in the channel that would bring the bottom (φ_{ch}) of an empty channel to a given Fermi level

$$N_0 = N_D^{loc}|_{\varphi_{ch}=\Phi_{ch}}. \tag{12}$$

Now, using the local-capacitance approximation we can write the following equation for the local value of φ_{ch} for sufficiently low values of N_D^{loc}:

$$\varphi_{ch} = \Phi_{ch} + \frac{e^2}{C}(N_0 - N_D^{loc}), \quad \text{if } N_D^{loc} < N_0, \tag{13}$$

where we take also the temperature equal to zero ($T=0$), i.e., there are no electrons above the Fermi level in the channel

$$n_{e0}^{loc} = 0, \quad \text{if } N_D^{loc} < N_0. \tag{14}$$

The situation is a bit more complicated, when $N_D^{loc} > N_0$, those regions of the channel will be filled by electrons. We can write the following equations for n_{e0}^{loc} and for φ_{ch}, screened by the channel electrons:

$$\Phi_{ch} - \varphi_{ch} = \frac{n_{e0}^{loc}}{\rho_{2D}}, \tag{15}$$

$$\Phi_{ch} - \varphi_{ch} = \frac{e^2}{C}(N_D^{loc} - N_0 - n_{e0}^{loc}). \tag{16}$$

Solving the Eqs. (15) and (16) and combining the solution with Eqs. (13) and (14), we get the following expressions for the channel-bottom electron potential energy:

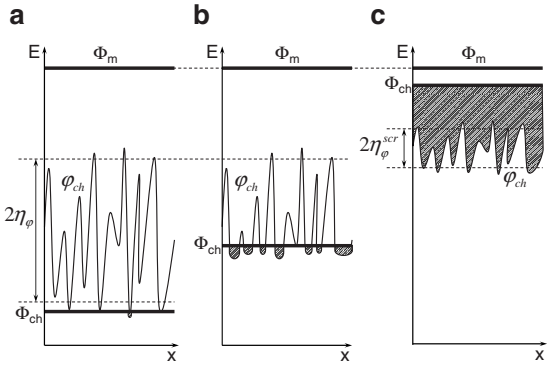

FIG. 9. Illustration to the nonlinear screening of the microscopical fluctuations of the electron potential energy in the channel for different values of the channel Fermi level (Φ_{ch}). Potential profile in the case of (a) depleted (low Φ_{ch}), (b) partly filled (intermediate Φ_{ch}), and (c) fully filled (high Φ_{ch}) channel.

$$\varphi_{ch} = \begin{cases} \Phi_{ch} + \dfrac{e^2}{C}(N_0 - N_D^{loc}) & \text{if } N_D^{loc} < N_0 \\ \Phi_{ch} - \dfrac{1}{1+\beta}\dfrac{e^2}{C}(N_D^{loc} - N_0) & \text{if } N_D^{loc} \geq N_0 \end{cases} \tag{17}$$

and for the electron concentration in the channel

$$n_{e0}^{loc} = \begin{cases} 0 & \text{if } N_D^{loc} < N_0 \\ \dfrac{\beta}{1+\beta}(N_D^{loc} - N_0) & \text{if } N_D^{loc} \geq N_0. \end{cases} \tag{18}$$

The electron screening is a local screening mechanism in the framework of the used local-capacitance approximation. The neighboring regions are not affected by the screening of a particular local fluctuation.

The above equations let us calculate the values of the screened and not-screened (by electrons) fluctuations of the electron potential energy in the channel. Equation (13) shows, that when the channel is fully depleted of electrons [$N_0 - N_D^{loc} \gg \eta_{ND}$, the channel Fermi level is low, see Fig. 9(a)], then the electron-potential-energy fluctuations could be described by the Gaussian distribution [since $\delta\varphi_{ch} \propto \delta N_D^{loc}$ in Eq. (13)] with the standard deviation given by

$$\eta_\varphi = \frac{e^2}{C}\eta_{ND} = 4\sqrt{\pi}\frac{d}{r}\frac{e^2}{\varepsilon}\sqrt{N_D}. \tag{19}$$

In the opposite case, when the Fermi level in the channel is high [$N_D^{loc} - N_0 \gg \eta_{ND}$, see Fig. 9(c)] and all the electron-potential-energy fluctuations are under the Fermi level, then it follows from the lower part of Eq. (17) that the screened channel-bottom fluctuations are also Gaussian, although with a different standard deviation

$$\eta_\varphi^{scr} = \frac{1}{1+\beta}\frac{e^2}{C}\eta_{ND} \overset{\beta \gg 1}{\approx} \frac{\eta_{ND}}{\rho_{2D}}. \tag{20}$$

We see that the fluctuations are suppressed by the factor of $1+\beta$ (which is ~ 10 in our structures) due to the electron screening, as compared to Eq. (19) but the electron-potential-energy fluctuations stay symmetric with respect to a certain average level and Gaussian in both cases. The screening is linear in both limiting cases.

In the intermediate case ($|N_D^{loc} - N_0| \lesssim \eta_{ND}$), $\delta\varphi_{ch}$ is not simply $\propto \delta N_D^{loc}$, the electron-potential-energy fluctuations are not Gaussian any more, they become strongly asymmetric, as we can see from Eq. (17). The screening is essentially nonlinear in this case: a part of fluctuations will be screened ($N_D^{loc} > N_0$) and a part will be not screened ($N_D^{loc} < N_0$). The latter fluctuations will have large amplitude, although the screened ones will be suppressed, see Fig. 9(b).

Now, let us define the radius of the fluctuations. We define it in such a way, that it maximizes the amplitude of the electron-potential-energy fluctuations in Eq. (19). Equations (9) and (19), on one hand, show that the amplitude of the fluctuations grows with the decrease in the radius of the fluctuations and the amplitude of the fluctuations is diverging in the limit $r \to 0$. On the other hand, the local-capacitance approximation, which was used to derive Eq. (19), fails in the limit $2r \ll d$. Therefore, we need to refine the approximation to determine an optimum radius.

For that purpose, we apply an approach similar to the linear "uniform cluster" approximation used by Kane,[22] where the fluctuations of fixed size were considered in a doped three-dimensional (3D) sample. We modify the approach for the case of 2D dopant layer and include the gate screening. The average electron potential energy created by a donor in a cluster S of radius r is defined in the model as the uniform average

$$\langle v \rangle = \frac{1}{S^2}\int_S v(\vec{R}_1 - \vec{R}_2)\mathrm{d}\vec{R}_1 d\vec{R}_2, \tag{21}$$

where v is the Coulomb potential energy of a donor screened by the gate

$$v(\vec{R}) = -\frac{e^2}{\varepsilon|\vec{R}|} + \frac{e^2}{\varepsilon\sqrt{(2d)^2 + |\vec{R}|^2}}, \tag{22}$$

where $\vec{R}$ is the coordinate in the plane of the δ layer. Calculation of $\langle v \rangle$ shows (we skip the calculation details here) that

$$\langle v \rangle \approx -1.7\frac{e^2}{\varepsilon r} \tag{23}$$

in the limit $r \ll 2d$ and $\langle v \rangle$ coincides with the local-capacitance approximation in the opposite limit $r \gg 2d$. The analysis of the standard deviation for the electron-potential-energy fluctuations ($\eta_\varphi^{un.cl.} = \eta_{ND} S\langle v \rangle$) in this case shows that $\eta_\varphi^{un.cl.}$ is a monotonously increasing function of r, when $r \to 0$, with

$$\eta_\varphi^{un.cl.}\big|_{r \ll 2d} \approx \max(\eta_\varphi^{un.cl.}) \approx 1.7\sqrt{\pi}\frac{e^2}{\varepsilon}\sqrt{N_D}. \tag{24}$$

It has been also shown in Ref. 22 that the uniform-cluster approximation, where the fluctuations with a fixed radius are considered only, underestimates the amplitude of the electron-potential-energy fluctuations, which are, generally speaking, determined by the fluctuations with all possible radii. For example, the Thomas-Fermi method,[22] where the fluctuations with different radii are taken into account, gives

the electron-potential-energy fluctuations of a factor of ≈ 2 larger as compared to the uniform-cluster approximation in the case of doped 3D samples, see.[22] Therefore, as a rough approximation, we choose the fluctuation radius in our local-capacitance approximation in such a way that $\eta_\varphi \approx 2 \max(\eta_\varphi^{un.cl.})$. Substituting Eqs. (19) and (24) into this relation, we get the optimum radius of

$$r = d. \tag{25}$$

The choice of the radius also fulfills the condition (10). In the following calculation we take into account such "optimum" fluctuations with the radius given by Eq. (25) only.

Further, we can calculate the average electron concentration (n_{e0}) in the channel. We average Eq. (18) over the distribution of the microscopical donor fluctuations in Eq. (8)

$$n_{e0} = \langle n_{e0}^{loc} \rangle = \int_0^\infty n_{e0}^{loc}(N_D^{loc}) P_{ND}(N_D^{loc}) dN_D^{loc}. \tag{26}$$

The electron-potential-energy fluctuations in the fully depleted channel are symmetric with respect to a certain average level. That means that the percolation threshold coincides with the average level. Since $\delta\varphi_{ch} \sim \delta N_D^{loc}$ in Eq. (13) and the fluctuations N_D^{loc} are symmetric with respect to N_D [see, Eq. (8)], then the percolation threshold is determined by the condition: $N_0 = N_D$. The critical average electron concentration (n_c) in the channel corresponding to the percolation threshold is [from Eqs. (18) and (26)]

$$n_c = \frac{\beta}{1+\beta} \int_{N_D}^\infty (N_D^{loc} - N_D) P_{ND}(N_D^{loc}) dN_D^{loc} = \frac{\beta}{1+\beta} \frac{\eta_{ND}}{\sqrt{2\pi}}. \tag{27}$$

The parameter β is $\gg 1$ in our structure and n_c becomes independent of β and also of the Coulomb energy in this limit. The independence of n_c of the Coulomb energy might seem strange, but this is not something unusual in the percolation problems,[23] when the density of the electron states is much higher than some characteristic inverse Coulomb energy. In our case, that corresponds to the condition $\beta \gg 1$, where β is a product of the 2D density of the electron states and a Coulomb term in Eq. (2).

Further, we can define a density of the "active" electrons above the percolation threshold as

$$n_{e0}^{act} = \begin{cases} 0 & \text{if } n_{e0} < n_c \\ n_{e0} - n_c & \text{if } n_{e0} \geq n_c. \end{cases} \tag{28}$$

Now, let us make some numerical assessments for our structures. The average donor density in our structures is $N_D \approx 7.2 \times 10^{12}$ cm^{-2}. That gives us $N_D \pi r^2 \approx 100$ for the average number of donors in a circle of the optimum radius $r=d$ and the condition (6) is satisfied. The standard deviation of the donor-density fluctuations is $\eta_{ND} \approx 7.5 \times 10^{11}$ cm^{-2}, according to Eq. (9). That means that $\eta_{ND} \ll N_D$ and the condition (7) is satisfied in the vicinity of the channel-depletion regime, when $n_{e0} \sim n_c$. The critical electron concentration in the channel at the percolation threshold is $n_c \approx 2.7 \times 10^{11}$ cm^{-2}, according to Eq. (27). The standard deviations of the electron-potential-energy fluctuations in the regime of fully depleted channel in Eq. (19) is $\eta_\varphi \approx 250$ meV. Such not-screened fluctuations have an unexpectedly large amplitude. Although the regime is not achievable in our structures, η_φ does describe the scale of the not-screened fluctuations in the regime of a partly filled channel, see Eq. (17) and Fig. 9(b). In the case of channel filled by electrons, the standard deviations of the fully screened electron-potential-energy fluctuations in Eq. (20) is $\eta_\varphi^{scr} \approx 28$ meV. The half width of 17 meV of the broadening of the ground subband assumed in the low-bias calculations is somewhat lower than η_φ^{scr} above. That could be explained by the filling of the first-excited subband in the low-bias regime. The filling of the next excited subband doubles the density of states in the channel, the effective parameter β will be a factor of two larger and, according to Eq. (20), the standard deviation for the screened fluctuations will be approximately one half of the value given above: $\eta_\varphi^{scr}/2 \approx 14$ meV. The latter value is already close the ground-subband broadening assumed in the low-bias regime. The broadening of the higher subbands is lower, this is probably because the corresponding wave functions are more delocalized with respect to the δ layer and less affected by the electron-potential-energy fluctuations.

The bias dependences of n_{e0}^{act} and n_{e0} calculated with Eqs. (26) and (28) are shown in Fig. 4. One can see that the percolation threshold is reached at the bias of 1 V in our structures, when $n_{e0}^{act} = 0$ and $n_{e0} = n_c$.

The δ-doped layers (although without gate) with similar donor density have been studied in Ref. 16 before. The calculations of the electron concentration at the percolation threshold in Ref. 16 gave $n_c \approx 10^{12}$ cm^{-2}, which is approximately a factor of ≈ 3 higher than that in our calculations. Since both our calculation method of n_c and that used in Ref. 16 could be considered as an order of magnitude assessments only, our calculation results are in reasonable agreement with Ref. 16. A somewhat lower calculated value of n_c in our case probably should be attributed to account of the asymmetry and of the non-Gaussian character of the microscopical potential fluctuations in the nonlinear-screening regime. As one can see from Eq. (17) and the illustration in Fig. 9(b), the potential fluctuations are strongly asymmetric in our model. A qualitatively similar strong asymmetry of the potential fluctuations has been also shown[23] to take place in the related not-gated structures, where the doping layer is a bit shifted with respect to 2D channel.

C. Tunnel current

Now, let us calculate the tunnel current between the gate and the channel with account of microscopical potential fluctuations described in the previous section. At low and negative biases, the electrons are tunneling between the metal gate and the lowest few subbands in the channel. An accurate self-consistent solution of the Schrödinger and Poisson equations is necessary in this case, as it is outlined in Sec. III. In the contrary, at large positive biases, the electrons are tunneling from the metal gate into the predominantly high-numbered (~ 50) 2D subbands. Therefore, we can treat the 2D subbands in the channel quasiclassically in the large-bias

regime. The equation for the local gate→channel tunnel current density (j_t^{loc}) can be written in the following form in this case

$$j_t^{loc}(\varphi_{ch}) = e\frac{\rho_{2D}}{2\pi\hbar}\int_{\varphi_{ch}}^{\Phi_m}(\Phi_m - E_\perp)T_{tun}(F(\varphi_{ch}),E_\perp)dE_\perp, \tag{29}$$

where $E_\perp$ is the electron energy in the channel (corresponding to the electron motion perpendicular to the barrier), T_{tun} is the barrier tunnel coefficient at the energy of the incident electron of $E_\perp$ and F is the electric field in the triangular barrier between the gate and the channel. The quasiclassical expression for T_{tun} in the two-band approximation is

$$T_{tun}(F,E_\perp) = \exp\left[-\frac{2\sqrt{2m^*}}{e\hbar}\frac{E_g^{3/2}}{F}G\left(\frac{\varphi_b}{E_g}\right)\right], \tag{30}$$

where

$$G(Z) = \int_0^Z \sqrt{Y(1-Y)}dY, \quad 0 < Z < 1,$$

$$= \frac{1}{4}[\sqrt{Z}\sqrt{1-Z}(2Z-1) + \arcsin(\sqrt{Z})], \tag{31}$$

$$\varphi_b = \varphi_b(E_\perp) = \varphi_{sch} + \Phi_m - E_\perp, \tag{32}$$

$$F = F(\varphi_{ch}) = \frac{\varphi_{sch} + \Phi_m - \varphi_{ch}}{ed}, \tag{33}$$

$\varphi_b(E_\perp)$ is the height of the triangular barrier for an electron incident on the barrier with the energy of $E_\perp$, φ_{sch} is the Schottky-barrier height relative to the Fermi level in the metal gate (Φ_m), m^* is the electron effective mass at the conduction-band bottom, E_g is the band-gap energy.

Further, we need to calculate the local tunnel-current density (j_t) averaged over the microscopical potential fluctuations in the channel, i.e., over the fluctuations of the barrier tunnel transparency as a consequence of the fluctuations of the electric field inside the barrier. The current is given by the equation

$$j_t = \int_{-\infty}^{\infty} j_t^{loc}[\varphi_{ch}(N_D^{loc})]P_{ND}(N_D^{loc})dN_D^{loc}, \tag{34}$$

where P_{ND} is the distribution function for the donor-concentration fluctuations in Eq. (8), j_t^{loc} is given by Eq. (29) and dependence of φ_{ch} on N_D^{loc} is described by Eq. (17).

Now, we calculate the value of j_t for our structures numerically. For every bias point, we calculate the potential-energy profile self-consistently for a given bias between the gate and the channel, by φ_{ch} we define the energy of the bottom of the ground subband in the channel. Then we find the value N_0 such that the Eq. (12) is satisfied. After that we can calculate the nonlinearly screened fluctuations of the electron potential energy with Eq. (17) and also the tunnel current in Eq. (34). The dependence of the tunnel current on the local bias in the channel is shown in Fig. 10. The tunnel current in Fig. 10 tends to saturation near and above the bias of the percolation threshold of 1 V (see Fig. 4). This is because the channel becomes depleted at such biases, the energy difference between Φ_m and the channel bottom saturates [see Fig. 9(a)] and that leads to the saturation of the tunnel current.

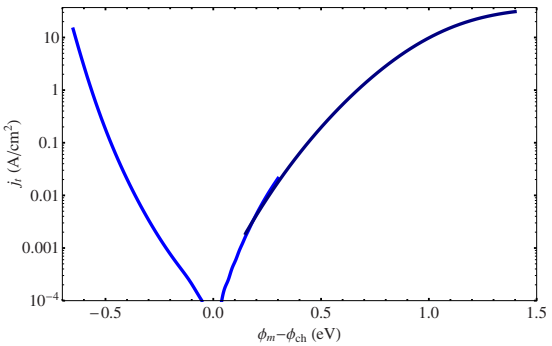

FIG. 10. (Color online) The light-blue line ($\Phi_m - \Phi_{ch} > 0.2$ eV) is the local tunnel-current density calculated with the large-bias model with averaging over microscopical potential fluctuations, as described by Eq. (34). The dark-blue line ($\Phi_m - \Phi_{ch} < 0.3$ eV) is the current density calculated with the low-bias model, here the tunneling is taking place to/from few lowest channel subbands only.

At low and negative biases the microscopical fluctuations in the channel are suppressed, therefore we neglect them and use the low-bias model for calculation of the tunnel current, as it is outlined in Sec. III B. The tunnel current calculated in this regime is also shown in Fig. 10.

D. Channel current

Now that we know the electron concentration in the channel and the tunnel current averaged over the microscopical fluctuations, let us consider the equations describing the electron flow along the channel and the corresponding macroscopical inhomogeneities. The channel current and the electron potential energy drop along the channel are described by the following set of equations:

$$j_{ch} = -n_{e0}^{act}(\Phi_{ch})\mu_0(\Phi_{ch})\frac{\partial\Phi_{ch}}{\partial x}, \tag{35}$$

$$\frac{\partial j_{ch}}{\partial x} = j_t(\Phi_{ch}), \tag{36}$$

where j_{ch} is the 2D channel current density per unity of the channel width, $\Phi_{ch}=\Phi_{ch}(x)$ is the local Fermi level in the channel, x is the coordinate along the channel with the zero chosen at the source edge of the gate. The first Eq. (35) is a material equation, which takes into account the conductivity due to the lowest subband in the channel with the local active 2D electron concentration of $n_{e0}^{act}(\Phi_{ch})$ and the mobility $\mu_0(\Phi_{ch})$. Equation (35) is used in the "large-bias model," when a large positive bias is applied to the structure. At low and negative biases, we replace Eq. (35) with the following equation:

$$j_{ch} = -[n_{e0}(\Phi_{ch})\mu_0^0 + n_{e1}(\Phi_{ch})\mu_1^0]\frac{\partial \Phi_{ch}}{\partial x}, \quad (37)$$

where μ_i^0 are the bias independent subband mobilities measured at zero bias. This equation is used in the calculations with a "low-bias model." The second Eq. (36) is the continuity equation, where $j_t(\Phi_{ch})$ is the local density of the tunnel current between the gate and the channel. $j_t(\Phi_{ch})$ has been calculated either with Eq. (34) in the case of large bias model or as it is outlined in the Sec. III in the low-bias regime.

The Eqs. (35) [or Eq. (37) and (36) were solved with the boundary conditions that $j_{ch}=0$ at the open source side of the structure at $x=0$ and $\Phi_m-\Phi_{ch}=eU_{ch\text{-}dr}$ at the drain edge of the gate, where $U_{ch\text{-}dr}$ is related to the total bias U applied between the gate and the drain Ohmic contact by (see schematic in Fig. 8)

$$U = U_{ch\text{-}dr} + U_{ch}^{op} + U_{edge}, \quad (38)$$

where $U_{ch}^{op}=j_{ch}L_{ch}^{op}/\sigma_{ch}^{op}$ is the voltage drop over the open (not gated) channel between the gate edge and the drain contact, σ_{ch}^{op} and L_{ch}^{op} are the conductivity (per square) and the length of the not-gated channel, U_{edge} is the voltage drop over the depleted and transitional regions at the drain edge of the gate between the gated and not-gated parts of the channel. Since the local capacitance approximation is not valid in the transitional region at the edge of the gate, we need to consider the region separately.

For assessment of U_{edge} we were assuming that $U_{edge}=F_{ch}L_{edge}$, here F_{ch} is the electric field along the channel under its drain edge, L_{edge} is the length of the depleted/transitional region. According to Ref. 24, the depletion length in a 2D channel (with the electron concentration as in our structures) at the edge of a gate is less than $\approx$20 nm even for the bias of $\sim$2 V between the gate and the 2D channel. The other relevant length scale for the transitional region is the gate-channel distance, which is also $\approx$20 nm in our structures. Therefore, we assume in the following that $L_{edge}\approx 30$ nm. Our calculations show that U_{edge} is always negligibly small, except for the current-saturation regime ($F_{ch}\sim F_{sat}$), where U_{edge} can amount to $\approx$0.15 V in our structures. The length L_{edge} also gives roughly the length scale of the edge region where the edge current (omitted in the above model) is injected into the channel in the current-saturation regime (above $\approx$0.9 V in Fig. 5).

We have chosen the dependence of the channel mobility in Eq. (35) on the Fermi level there in the form

$$\mu_0(\Phi_{ch}) = \mu_0^0\left[1+\exp\left(\frac{\Phi_m-\Phi_{ch}-430\ \text{meV}}{90\ \text{meV}}\right)\right]^{-1}. \quad (39)$$

The parameters in the correction factor $(\ldots)^{-1}$ in Eq. (39) are chosen in such a way, that, first, the mobility tends to zero at large biases, when the channel is depleted and its electron concentration is getting lower than the critical value at the percolation threshold; second, μ_0 tends to μ_0^0 at low biases; third, the values of the saturation currents at large applied biases agree well with the measurements for both samples d and e, see Fig. 5. Calculating the electron concentration for given Φ_{ch}, we can illustrate the dependence of the mobility on the electron concentration in the channel, see Fig. 11. The approximation in Eq. (39) is discussed in more details below.

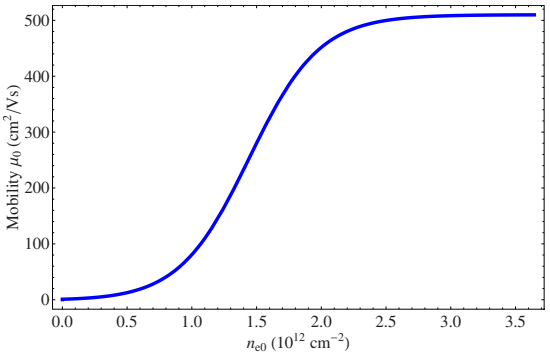

FIG. 11. (Color online) Mobility in the ground subband vs electron concentration in the subband as described by Eq. (39).

E. Comparison with measured characteristics

The calculated *I-V* and differential resistance characteristics of the structures are shown in Figs. 5 and 6, they are in good quantitative agreement with the measurement results in the full measurement range. Here we have used low-bias model at the biases below $\sim$0.3 V and we have used the large-bias model at higher biases. Somewhat overestimated value of the calculated differential resistances at around $\gtrsim$1.2 V is probably due to neglected additional "edge" tunnel current in the theoretical model. The edge current would contribute to a slow growth of the current in the saturation region in Fig. 5 and corresponding decrease of the large-positive-bias differential resistance in Fig. 6 at the biases above $\approx$1.2 V. The calculated voltages at the source and rho contacts are shown in Fig. 7, they are also in quite good agreement with the measured characteristics.

F. Inhomogeneities at large biases

In this section we will be discussing the potentials, electron concentrations, currents, etc. averaged over microscopical fluctuations discussed in Secs. V B and V C. At large positive biases, the distribution of the tunnel current becomes essentially macroscopically inhomogeneous along the gate. The features, corresponding to the onset of tunneling to different subbands (see Fig. 3), in the spectrum are washed away in this case. One can even come to a situation, when the total tunnel current flowing through the structure is determined mostly by a small part of the structure at the end of the gate, which is close to the drain Ohmic contact. Figure 12 illustrates strong macroscopical inhomogeneities of $\Phi_{ch}(x)$, total channel current $I_{ch}(x)=Wj_{ch}$ (W is the channel width), $n_{e0}(x)$ and $j_t(x)$ for the samples e and d in the situations close to the current saturation. We were assuming here that the electric field along the channel under the drain edge of the gate reaches $F_{sat}=50$ kV/cm. The value of F_{sat} has been roughly chosen in such a way, that F_{sat} times the mobility of $\sim$100 cm^2/Vs is close to the electron saturation velocity of

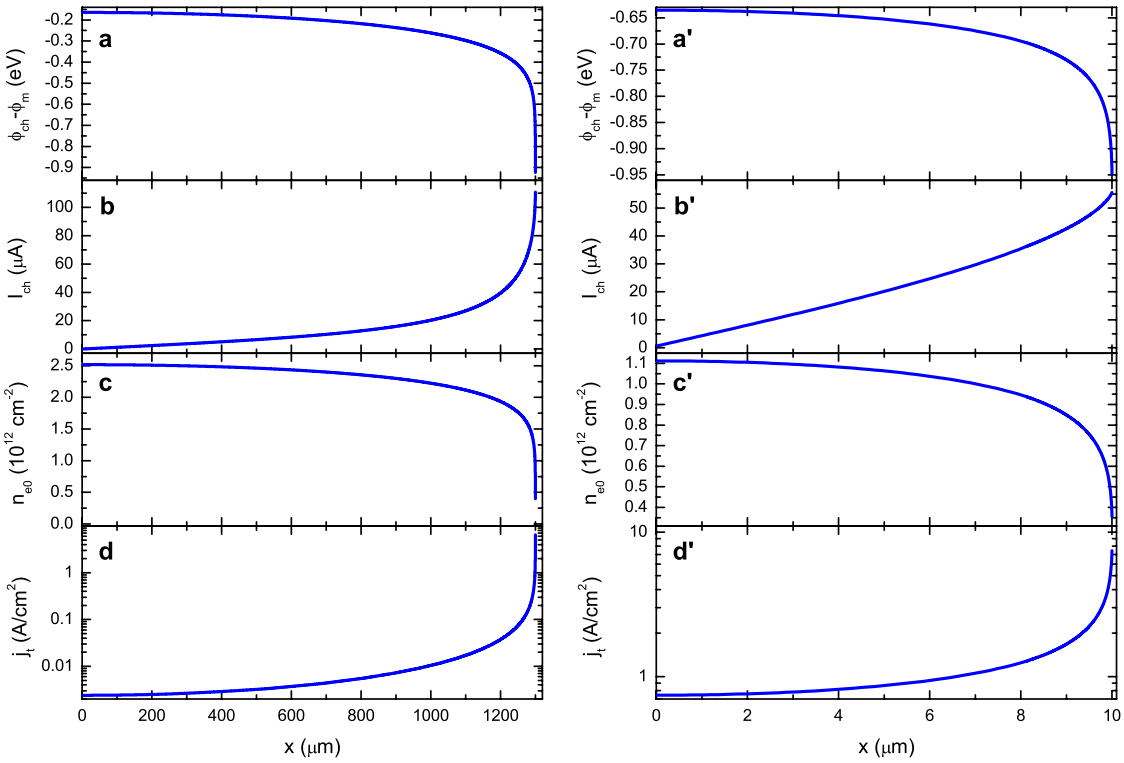

FIG. 12. (Color online) Calculated nonhomogeneous distributions of the channel Fermi level Φ_{ch} [Figs. (a) and (a′)], the channel current I_{ch} [Figs. (b) and (b′)], the electron concentration n_{e0} in the lowest subband [Figs. (c) and (c′)] and the tunnel-current density j_t [Figs. (d) and (d′)] in the current-saturation regime. The figures on the left (right) side show the plots for the sample e (sample d). Here we have chosen the biases applied to the structures in such a way that the electric field along the channel under the drain (right) edge of the gate is 50 kV/cm.

$\sim 5\times 10^6-10^7$ cm/s. As our calculations show, the choice of the particular vale of F_{sat} does not have large impact on the calculated characteristics of the structures. The ends of the calculated curves at positive biases in Figs. 5–7 correspond to the condition $F=F_{sat}$. At the very right edges of the gates the electron concentration in the channels is getting close to the minimum achievable value $n_{e0}\rightarrow n_c$, see Fig. 12. One can see in Fig. 12 that the tunnel-current density grows by almost four orders of magnitude toward the right side of the structure e, where the Ohmic contact to the channel is placed, and more than half of the total current of the structure is injected into the channel through the last 50 μm of the gate, although the whole structure is more than 20 times longer than that. One can also see that the voltage drop along the channel under the gate of sample e is pretty large, it is $\approx$0.8 V. The inhomogeneities are also significant in the structure d with the short gate. Here the tunnel current is changing by an order of magnitude along the gate and the voltage drop along the channel under the gate is as large as $\approx$0.3 V. In such a way we see that the macroscopical inhomogeneities can be very significant in the large-bias regime.

G. Mobility at large biases

As we have mentioned above in Sec. V D, the dependence in Eq. (39) of the mobility on the Fermi level (or on the electron concentration) in the channel is chosen in such a way, that the mobility is getting very low at large biases, when the electron concentration in the channel is approaching the percolation threshold. The choice of the mobility dependence on the electron concentration has significant influence on the current-voltage characteristics at large biases, especially on the value of the saturation current. For example, if we would take the electron mobilities in the channel as bias independent and equal to the mobilities measured at zero bias, then we would get the calculated saturation currents for both samples d and e by approximately factor of four higher than the measured values. Therefore, the measured value of the saturation current gives an indirect evidence for a decrease of mobility at large biases (at low electron densities in the channel). Qualitatively, a high mobility at large biases makes the region close to the drain edge of the gate with large voltage drop over the barrier wider. The tunnel current is large in the region. Consequently, the total current of the structure gets higher.

We could measure directly the mobility and the channel conductivity in our structures at low biases only, the measurements of the mobility at large biases were not possible because of relatively high tunnel current and appearance of macroscopical inhomogeneities. There are some, although just few, reports[15,16] in the literature, where the behavior of the conductivity and mobility in the δ-doped layers with high doping level has been studied in the past. The investigations have been done on not-tunnel structures. The conductivity of the 2D channel was going to zero at $n\approx 10^{12}$ cm^{-2} in the structures investigated in Ref. 15, where the δ-n-doping level

was $\approx 1.6\times 10^{12}$ cm^{-2}, with the conductivity of the channel rapidly increasing at higher electron concentration. In Ref. 16 it was shown that the mobility of the 2D channel with δ-n doping at the level of $\approx 6.6\times 10^{12}$ cm^{-2} is decreasing rapidly already at the electron concentration of $n\approx 2\times 10^{12}$ cm^{-2} and it tends to zero at $n\approx 10^{12}$ cm^{-2}. We have chosen the dependence of the mobility on the electron concentration in the channel defined by Eq. (39) and shown in Fig. 11 to be similar (except for two differences) to the one reported in Ref. 16 in the δ layers with similar doping level. One difference is that the electron mobility at high electron concentrations in our samples is somewhat lower than that in Ref. 16 that could be due to a different electron confinement in our structure. The other difference is that the mobility is getting very low in our approximation in Eq. (39) at the electron concentrations which are by $\approx 5-7\times 10^{11}$ cm^{-2} lower than that in Ref. 16. That is due to a lower value of the electron concentration at the percolation threshold in our model for our structures. Our value is a factor of three lower than $\approx 10^{12}$ cm^{-2} reported in Ref. 16 and that explains the shift of the mobility drop toward lower electron concentrations in Eq. (39) and Fig. 11, as compared to that in Ref. 16.

At this point we have to mention that both in our work presented here and in Refs. 15 and 16 there are no direct measurements of the electron concentration in the channel in the regime, when the channel is getting depleted. Instead, different characteristics of the structures were measured vs bias while a relation between the bias and the electron concentration in the channel was always established on the basis of self-consistent calculations of the potential profile of the 2D channels. Further, good agreement between different measured and calculated characteristics was giving indirect support to the calculated values of the electron concentration both in our and in the cited works. Nevertheless, the values of the electron concentration are not known for sure. The outcome of the electron-density calculations strongly depends on the assumptions made. For example, the density of active donors in the channel is usually a poorly defined parameter but it has strong influence on the electron concentration in the channel. Also, the assumptions made in the modeling of the microscopical charge fluctuations have an impact on the calculated value of the electron concentration, e.g., in the regimes close to the percolation threshold. As we have mentioned in Sec. V B, the nature of the calculation approaches used in our work and in Ref. 16 gives an order of magnitude assessment for the electron concentration at the percolation threshold only. In view of such uncertainties, our approximation in Eq. (39) and Fig. 11 for the dependence of mobility on applied bias (and on the electron concentration) agrees reasonably well with the earlier publications.

The rapid decrease in the conductivity and mobility in the heavily doped δ layer at nonzero electron concentration ($\sim 10^{12}$ cm^{-2}) was attributed to disorder-induced metal-insulator transition in Refs. 15 and 16. To support that, the temperature dependence of conductivity and other characteristics of the δ layer were extensively investigated in Ref. 16. We believe that the nature of the mobility decrease [Eq. (39) and Fig. 11] at low electron concentrations in our structures should be also related to the disorder-induced metal-insulator transition. Although the mobility should be changing as a power law[25,26] close to the percolation threshold, this behavior is a too subtle effect to be investigated/identified in our structures, since it is limited to close vicinity ($|n_{e0}-n_c| \ll n_c$) to the percolation threshold only.[25] As one can see in Fig. 12, the electron concentration in the channel is changing in a wide range ($|n_{e0}-n_c| \gtrsim n_c$) close to the current saturation regime (when a part of the channel is approaching the percolation threshold) in our structures even with the shortest gate (type d). Additionally, the electric field in the depleted parts of the channel in our structures must be very strong, therefore the usual percolation theory[25] has limited applicability in this case. Consequently, a rough (exponential) model in Eq. (39) and Fig. 11 seems to be a reasonable approximation for our structures.

VI. CONCLUSIONS

In the present paper we were investigating the behavior of the tunnel δ-doped Schottky structures with 2D channel in the regime of large bias applied between the gate and the channel. The measurements reveal a number of peculiar features in the I-V and other characteristics at large applied biases. To describe the features, we have developed a model which takes into account both microscopical fluctuations of the donor density in the δ layer and the macroscopical inhomogeneities due to the current-spreading effects. Considering the microscopical donor-density fluctuations, we take into account the linear gate screening, nonlinear screening by the electrons in the channel, percolation effects, the influence of the fluctuations on the tunnel current, etc. Further, we identify the local (macroscopical) depletion of the channel as the bottleneck leading to the saturation of total current, to the increase in the differential resistance and to the freezing of the potential profile along the channel at large biases. Our measurements and calculations indicate that the channel is getting locally insulating due to the disorder-induced metal-insulator transition in our structures, when the electron concentration in the channel is still relatively high ($\approx 3\times 10^{11}$ cm^{-2}). The calculated tunnel characteristics of the structures are in good quantitative agreement with the measured ones at both low and large applied biases.

ACKNOWLEDGMENTS

The work was supported by RFBR (Grants No. 09-02-01159, No. 08-02-00206a, and No. 07-02-92171-PICS-a) and by RAS. We are grateful Yu. V. Fedorov and A. S. Bugaev for preparation of the samples and to M. S. Kagan for stimulating discussions and critical comments.

[1] M. Zachau, F. Koch, K. Ploog, P. Roentgen, and H. Beneking, Solid State Commun. **59**, 591 (1986).
[2] I. N. Kotel'nikov, V. A. Kokin, Y. V. Fedorov, A. V. Hook, and D. T. Talbaev, JETP Lett. **71**, 387 (2000).
[3] I. N. Kotel'nikov and S. E. Dizhur, JETP Lett. **81**, 458 (2005).
[4] I. N. Kotel'nikov, S. E. Dizhur, M. N. Feiginov, and N. A. Mordovets, Semiconductors **40**, 818 (2006).
[5] E. M. Dizhur, A. N. Voronovsky, A. V. Fedorov, I. N. Kotel'nikov, and S. E. Dizhur, JETP Lett. **80**, 433 (2004).
[6] M. N. Feiginov and I. N. Kotel'nikov, Appl. Phys. Lett. **91**, 083510 (2007).
[7] M. N. Feiginov, Appl. Phys. Lett. **81**, 930 (2002).
[8] D. C. Tsui, Phys. Rev. Lett. **24**, 303 (1970).
[9] E. L. Wolf, *Principles of Electron Tunneling Spectroscopy* (Oxford University Press, Oxford, 1985).
[10] T. Ando, A. B. Fowler, and F. Stern, Rev. Mod. Phys. **54**, 437 (1982).
[11] A. Y. Cho and P. D. Dernier, J. Appl. Phys. **49**, 3328 (1978).
[12] A. J. North, E. H. Linfield, M. Y. Simmons, D. A. Ritchie, M. L. Leadbeater, J. H. Burroughes, C. L. Foden, and M. Pepper, Phys. Rev. B **57**, 1847 (1998).
[13] J. D. Zimmerman, E. R. Brown, and A. C. Gossard, J. Vac. Sci. Technol. B **23**, 1929 (2005).
[14] E. Abrahams, S. V. Kravchenko, and M. P. Sarachik, Rev. Mod. Phys. **73**, 251 (2001).
[15] A. Zrenner, Ph.d. thesis, Technische Universität München, 1987.
[16] T. Schmidt, S. G. Müller, K. H. Gulden, C. Metzner, and G. H. Döhler, Phys. Rev. B **54**, 13980 (1996).
[17] J. W. Conley and G. D. Mahan, Phys. Rev. **161**, 681 (1967).
[18] I. N. Kotelnikov, D. K. Chepikov, E. G. Chirkova, and A. Y. Shulman, Sov. Phys. Semicond. **21**, 1123 (1987).
[19] W. I. Wang, J. Vac. Sci. Technol. B **1**, 574 (1983).
[20] C. Barret and J. Massies, J. Vac. Sci. Technol. B **1**, 819 (1983).
[21] M. Shur, *Physics of Semiconductor Devices* (Prentice-Hall, Englewood Cliffs, 1990).
[22] E. O. Kane, Phys. Rev. **131**, 79 (1963).
[23] A. L. Efros, F. G. Pikus, and V. G. Burnett, Phys. Rev. B **47**, 2233 (1993).
[24] L. I. Glazman and I. A. Larkin, Semicond. Sci. Technol. **6**, 32 (1991).
[25] B. I. Shklovskii and A. L. Efros, *Electronic Properties of Doped Semiconductors*, Springer Series in Solid-State Sciences Vol. 45 (Springer, Berlin, 1984).
[26] Y. Meir, Phys. Rev. Lett. **83**, 3506 (1999).